Signal Delay Effects of Solid Dielectrics on Time-of-Flight Measurements in GIS

Glenn Behrmann, Kris Wyss, Jonas Weiss, Markus Schraudolph
ABB Switzerland Ltd., High Voltage Systems
Brown Boveri Strasse 5
CH-8050, Zürich-Oerlikon, Switzerland

Stefan Neuhold
Fachkommission für Hochspannungsfragen (FKH)
FKH-Versuchsstation, Voltastrasse 9
CH-8044, Zürich, Switzerland

and **Jasmin Smajic**
University of Applied Sciences of Eastern Switzerland (HSR)
Institute for Energy Technology (IET), Oberseestrasse 10
CH-8640 Rapperswil, Switzerland

ABSTRACT
So-called 'time-of-flight' (TOF) measurements have been employed for locating PD sources within GIS for over 20 years. Portable digital sampling oscilloscopes have now become available for reasonable cost whose input rise-times, bandwidths, and sampling rates are theoretically sufficient to provide spatial resolution within approximately 10 centimeters. However, contrary to first impressions, GIS does not present an ideal propagation environment for GHz bandwidth radio frequency (RF) signals; many factors act to prevent reaching such high spatial resolution. In both laboratory measurements and field simulations, the authors have recently observed that solid dielectric insulators in the signal propagation path affect the accuracy of the location determination. Therefore, it is important to take the delay effects of solid dielectrics into account in order to increase accuracy of TOF measurements. To this end, comparison measurements were made on a short section of GIS which clearly demonstrate the delay time effects as UHF signal pass through solid insulators. In addition, a sophisticated finite elements (FE) RF model was created for the same section of GIS in order to simulate electromagnetic wave propagation within it. The simulation results obtained were compared against the measurements for validation purposes. In addition, results from a practical on-site measurement are presented along with suggestions for others working in the field.

Index Terms - **Partial discharge, time-of-flight measurement, gas insulated switchgear, numerical field simulations.**

1 INTRODUCTION

THE so-called time-of-flight (TOF) measurement technique has been employed for more than 20 years for locating partial discharge (PD) sources inside gas-insulated switchgear (GIS), particularly on site [1-8]. With increasingly complex assembly units being built and tested in the factory, TOF measurements are also being employed there more often than in the past. By being able to precisely locate the PD source, overall quality is enhanced and costs are reduced, because the repairs take less time and less material needs to be replaced.

A conceptual drawing of the set-up used for carrying out TOF measurements is sketched out in Figure 1, with the location of the PD source being determined based on a calculation made using equation (1) [5, 7, 8]. This has usually been based on the assumption that the velocity of propagation of the electromagnetic traveling waves (resulting from the fast rise-time PD pulses) is or near c, the speed of light in a vacuum, and that it is uniform over the TOF path.

$$d = (D - 0.3t)/2 ,\ \ 0 \le d \le D \tag{1}$$

Manuscript received on July 31, 2015 in final form 6 October 2015, accepted 12 October 2015.

DOI: 10.1109/TDEI.2015.005535

A digital sampling oscilloscope (DSO) with adequate bandwidth and sampling rate (e.g. 1-2 GHz, 2-10 GS/s, resp.) is connected via equal-length cables (typically including RF pre-amplifiers, not shown in Fig. 1) to two PD sensors near the PD defect. The operator then adjusts the DSO to obtain the difference in the time-of-arrival of the two signals as accurately as possible. The PD source location is calculated based on Equation (1) as being distance *d* from the PD sensor from which the signal arrives first, with *d* and *D* in meters and where time *t* is the measured difference in time-of-arrival in nanoseconds.

Although the concept appears simple, obtaining an accurate measurement of *t* can be very challenging if the PD signal is weak or there is a high level of background interference – in other words, in conditions of poor signal-to-noise ratio (SNR). Ambiguity in determining the precise moment when the incoming signal arrives leads to imprecise values of *t* which in turn translates directly to errors in the location calculation. (The authors intend to explore some of these issues further in future work.)

Although the actual velocity of propagation in air or SF6 gas is very slightly lower owing to the difference in permittivity ε between vacuum and gas [9], the errors introduced by these differences are very small and may be neglected in the case of practical TOF measurements. The presence or number of insulators (spacers) in the TOF path was also largely ignored ignored till now, even though their coefficient of permittivity ε is much higher. However, recent TOF measurements made by the authors showed the latter assumption to be a potential source of error, both in the laboratory and on site. In the latter case, an error was made during a TOF measurement which was later determined to result from neglecting the lower velocity of propagation through solid insulation in the measurement path. This case, together with similar anomalies noticed during other TOF measurements, motivated the work presented here.

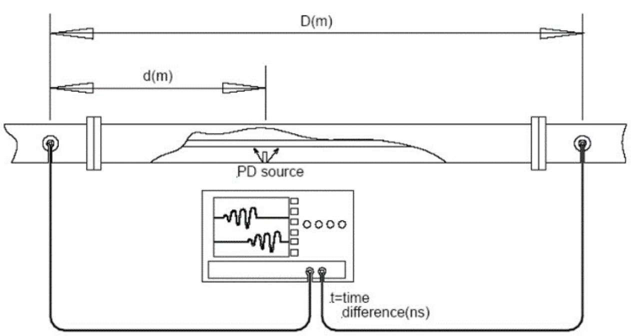

Figure 1. Conceptual sketch of TOF measurement with DSO connected with equal-length cables to two PD sensors. The time difference *t* and the distances *d* and *D* correspond to Equation (1).

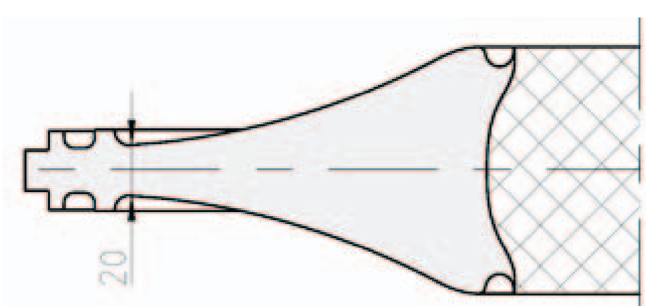

Figure 2. GIS barrier insulator profile showing variation in thickness is depicted. The effect on propagation velocity cannot be accurately modelled using only a simple cylindrical (disk) geometric shape.

Figure 3. The measurement set-up used to determine time delay effects of 5 insulators in series.

This work started by thinking about the influence of the epoxy resin insulators on the electromagnetic wave velocity, i.e. asking the question: could their presence in the TOF measurement path significantly affect location accuracy? The velocity of propagation in a dielectric is given by the following equation [10]:

$$v_w = \left(\mu_r \mu_0 \varepsilon_r \varepsilon_0\right)^{-1/2} \tag{2}$$

It can be seen in equation (2) that ε_r is the only parameter that has a significant effect on the wave velocity in solid dielectrics (e.g. filled epoxy), as the relative permeability μ_r of non-ferromagnetic materials is generally accepted as 1. Typical values are $\varepsilon_{epoxy} = 4.2$ and $\varepsilon_{SF6} = 1.0021$.

For example: when making a TOF measurement, if an epoxy resin disk insulator having a uniform width of 5 cm were present on one side of the measurement path but not on the other, the result of the location determination will be off by approximately 10 cm, based on the assumption the electromagnetic wave velocity is *c*, 30 cm/ns [3, 8]. However, barrier insulators are not typically a simple disk of uniform width, but instead vary significantly across their diameter as shown in Figure 2. At this stage it was not obvious how this variation in thickness would affect the propagation delay, so it was decided to temporarily abandon analysis and try to measure the delay effect instead.

After a first attempt to measure the delay effects of a single barrier insulator resulted in delay times which were deemed imprecise, it was decided to construct a measurement set-up which allowed measurement of the delay effect of five barrier insulators in series. In addition, a detailed 3D finite element (FE) radio-frequency (RF) model of the set-up was developed to see whether results similar to the measurements could be obtained.

We hope to contribute to the understanding of these effects in three ways: (a) to reveal the signal delay effects of insulators and their significance for TOF-measurements, (b) to investigate the effect in detail using 3-D FEM simulation models, and (c) to illustrate the effects described by presenting a practical on-site measurement example.

2 PRACTICAL DELAY MEASUREMENTS

The oscilloscopes used for the measurements have sampling rates of 10 GS/s. If we assume we require a minimum of 2 samples to establish a discernible rising edge (this is a purely theoretical assumption), this corresponds to a distance of a few centimeters; thus it would be difficult to accurately determine the delay effect of a single insulator. This was confirmed by simple laboratory experiments. To get a clearer result, we constructed the measurement set-up containing five barrier insulators in series shown in Figure 3.

Five epoxy-resin barrier (closed) insulators were installed between two UHF PD sensors with a third sensor on one end of the set-up used to inject a fast rise-time (< 130 ps) pulse from a commercially available GIS calibrator. The top photo of Figure 3 shows the entire set-up with the measurement equipment on a mobile rack, the bottom photo is a close-up of the signal generator positioned at the start of the measurement path. The measurement set-up was used for three separate measurements: one containing the five barrier insulators, one containing only a continuous inner conductor of standard diameter, and one containing the contact and field electrode assemblies normally included with each barrier insulator (i.e. 'all the metal but no epoxy'). The latter was a check to determine whether just the contact assemblies and field electrodes themselves make a measureable contribution to the signal delay. Use of the same standard insulator positioning rings for each measurement guaranteed that the exact same length between the TOF sensors was maintained.

During the measurement the GIS was filled with ambient air at atmospheric pressure instead of SF_6. The difference in the dielectric constant ε at 1 bar absolute pressure between air and SF_6 is insignificant and can therefore be neglected for the purpose of this measurement; we are looking only for the relative differences in propagation delay.

TOF measurements were carried out for the three configurations described above using a LeCroy model 204 MXiA digital sampling oscilloscope (2 GHz input bandwidth, 10 GS/s sampling rate). The results of the different time delays measured show by how much the electromagnetic wave is delayed by the insulator. The distance between the two sensors over which the difference in time-of-arrival was measured was 195 cm. With five identical barrier insulators installed, the TOF result was approximately 7.4 ns, and without the barrier insulators installed, the TOF time was 6.6 ns, resulting in a difference of approximately 0.8 ns. The time delay measured with only the contact assemblies installed was measured at 6.62 ns – in other words, essentially the same value as measured with the single continuous inner conductor, well within a reasonable measurement tolerance.- This means that one barrier insulator of this type produces a time delay of approximately 0.16 ns. Assuming the velocity of propagation c – approximately 30 cm/ns – an insulator not accounted for along a TOF path could result in a localization error of approximately 4.8 cm. While this may seem insignificant, it could be sufficient to be off by one compartment. Furthermore, the signal delay effects are compounded as the distance through which the TOF signals propagate through solid dielectric material increases. This will be shown in the practical example described below.

A second result of this laboratory measurement is that it also showed the influence of the shape of the insulator. The speed of the electromagnetic wave in epoxy is 14.6 ns/cm, based on equation (2). If we calculate backwards using the measured time delay of 0.16 ns/insulator, the theoretical width of the insulator comes out to be approximately 2.3 cm, which corresponds closely to the narrowest section of the insulators used for the experiment. In other words, the electromagnetic wave essentially traverses the path of least resistance, as would be expected. Note that no efforts were made to limit the effects of higher-order modes; the test was carried out in a simple, straightforward manner, typical of actual on-site conditions.

3 3-D FEM FIELD SIMULATION MODEL

Propagation of electromagnetic waves in GIS can presently be simulated in 3-D based on CAD-data (ProE) of the GIS in its full geometrical complexity. For the simulations presented in this paper, the following initial boundary value problem (IBVP) was considered [11]:

$$\nabla \times \left(\frac{1}{\mu_r} \nabla \times \vec{A} \right) + \mu_0 \sigma \frac{\partial \vec{A}}{\partial t} + \mu_0 \varepsilon_0 \left(\varepsilon_r \frac{\partial^2 \vec{A}}{\partial t^2} \right) = 0 \text{ in } \Omega \subseteq \mathrm{R}^3 \quad (3)$$

$$\vec{n} \times \vec{A} = 0 \text{ over } \partial_{PEC} \Omega \subseteq \mathrm{R}^2 \quad (4)$$

$$\vec{n} \times \left(\frac{1}{\mu_r \mu_0} \nabla \times \vec{A} \right) = 0 \text{ over } \partial_{PMC} \Omega \subseteq \mathrm{R}^2 \quad (5)$$

$$-\vec{n} \times \left(\frac{1}{\mu_r} \nabla \times \vec{A} \right) - \frac{\mu_0}{Z_{PORT}} \frac{\partial}{\partial t} \vec{n} \times \left(\vec{n} \times \vec{A} \right) =$$

$$\frac{2\mu_0}{Z_{PORT}} \vec{n} \times \left(\vec{n} \times \vec{E}_0 \right) \text{ over } \partial_{PORT} \Omega \subseteq \mathrm{R}^2 \quad (6)$$

$$\vec{A} = 0 \text{ for } t = 0 \text{ in } \Omega \subseteq \mathrm{R}^3 \quad (7)$$

where A is the vector magnetic potential, μ_0 is the magnetic permeability of vacuum, μ_r is the relative magnetic permeability of the material, ε_0 is the electric permittivity of vacuum, ε_r is the relative electric permittivity of the material,

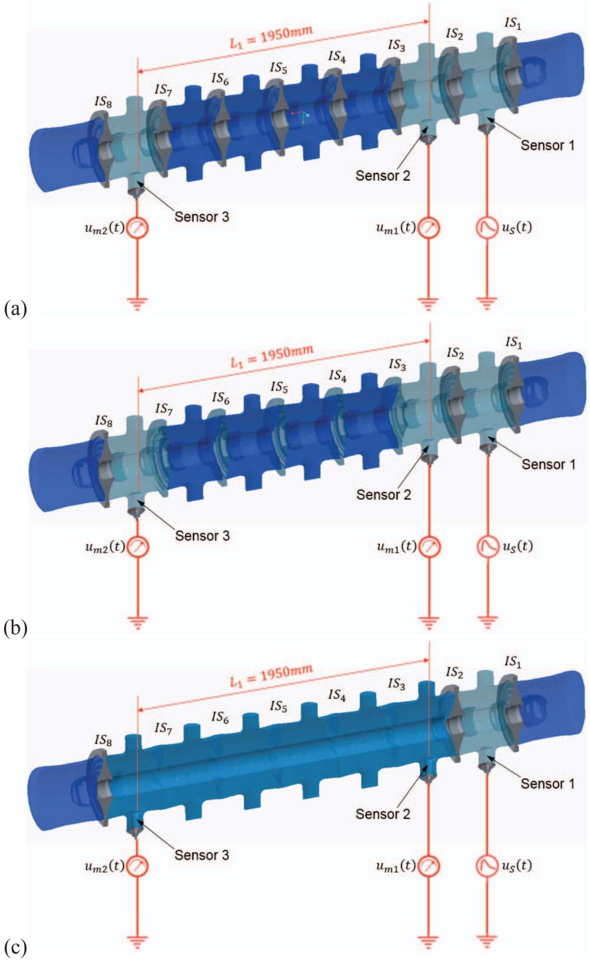

Figure 4. Three different simulated models are depicted: (a) Model 1 – the model with all the insulators in place (ε_r=4); (b) Model 2 – geometrically same as Model 1 but insulators IS3 – IS7 are modeled as SF6 (ε_r=1); (c) Model 3 – the insulators IS3-IS7 and the corresponding electric shields are replaced by a straight, end-to-end cylindrical conductor.

Ω is the 3-D volume of the GIS in which electromagnetic waves propagate, $\partial_{PEC}\Omega$ is the perfect electric conductor boundary (the outer surfaces of all conductors), $\partial_{PMC}\Omega$ is the perfect magnetic conductor boundary (the GIS symmetry, if any), $\partial_{PORT}\Omega$ is the port boundary through which the model's sensors are connected with the source (sensor 1) and the oscilloscope's inputs (sensors 2 and 3), Z_{PORT} is the wave impedance after the port boundary, and E_0 is the known source electric field at the source port, produced by the pulsed voltage source connected to it.

The above IBVP (3)-(7) is solved by using the modern vector finite element method [11] implemented in the commercial field solver COMSOL [12]. Three different 3-D models presented in Figure 4 were simulated.

The models presented in Figure 4 precisely correspond to the actual measurements taken as described above and to the set-up shown in Fig. 3. They are defined in such a way that they reveal the signal delay caused by the insulators. In Model 1, all five insulators are installed in series, causing the wave propagation delay. In Model 2, insulators 3-7 are removed, but the corresponding contact assemblies and shield electrodes are left in place. Finally, Model 3 only contains one long, continuous cylindrical inner conductor as used in the corresponding measurement; the FEM mesh of Model 3 is shown below in Fig. 6. The shape of the source impulse used as an excitation in all of the simulation models is shown in Fig. 5, based on a measurement of the actual pulse using the same digital oscilloscope used for the TOF measurements.

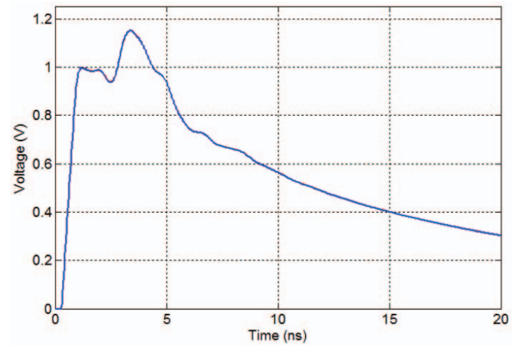

Figure 5. Plot showing the impulse shape of the voltage source attached to Sensor 1 of the modeled measurement set-up structure. The rise-time used for the simulation was set to 1ns, although shorter rise-times could be also used; see text.

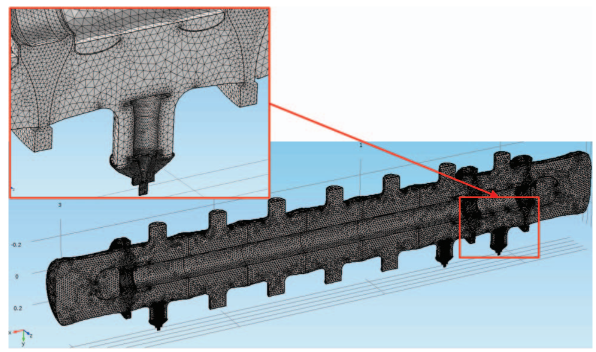

Figure 6. The 3-D tetrahedral mesh of Model 3 is shown. The mesh consists of 2'076'782 linear tetrahedrons resulting in a linear system of equations with 2'520'012 unknowns.

For the simulations, the rise-time of the impulse was set to 1 ns. The reason for this is a compromise in terms of the accuracy of the time-of-flight simulation vs. the CPU-time required. If the impulse rise-time shown in Figure 5 would be set to a shorter value, the time step of the simulation would need to be shorter. This in turn increases the number of simulation steps needed to cover the required simulation time which would dramatically increase the CPU time and memory required to perform each simulation. For the simulations performed here, the time window was 20 ns with step size of 0.05 ns; CPU time was 1:58:32 running on a multicore PC [Intel(R) Xeon(R) CPU E5-2670 0 @ 2.60 GHz (8 cores), with 128 GB RAM]..

To show the influence of the insulators, the simulation results of Model 1 and Model 3 are compared in Figure 7. The absolute value of the electric field is shown visualized in a sequence of moments of time. The increase in signal delay of Model 1 due solely to the effect of the insulators is clearly evident.

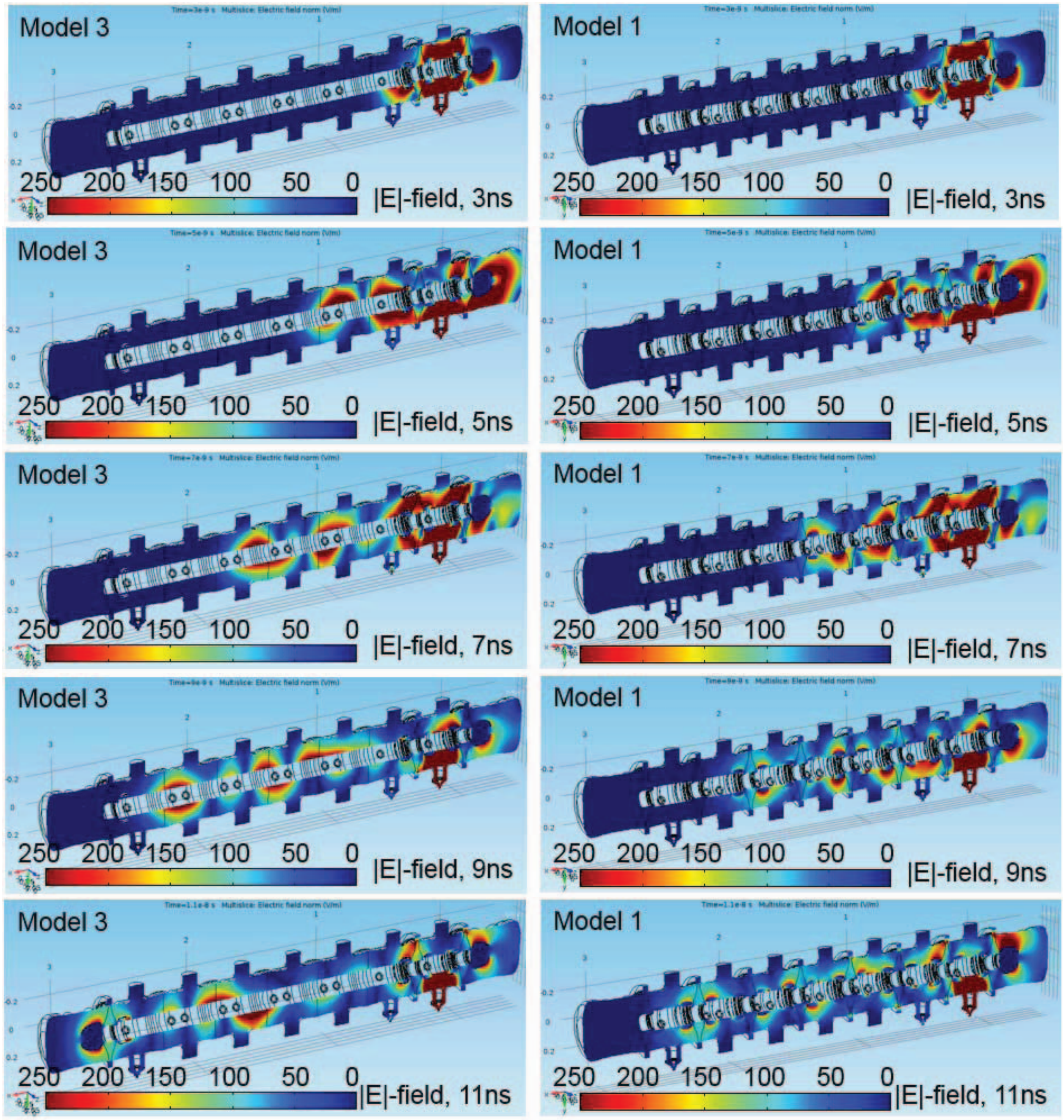

Figure 7. The impulse propagation in Model 3 (left) and Model 1 in a sequence of moments of time is shown. The absolute value of the electric field over the symmetry plane of the GIS arrangement is depicted. The signal delay of Model 1 compared to Model 3 is evident. The only difference between Model 1 and 3 is the lack or presence of the barrier insulators.

The electric field signals illuminating the sensors are integrated to obtain the voltage at the sensor outputs. The resulting time-of-arrival values (Δt) are shown in Figure 8. A comparison of the TOF-values shown in Fig. 8 reveal an excellent agreement with the actual measurements. The voltage waveforms have similar shapes at the beginning of the simulation time, but later on, the simulation and measurements begin to deviate from each other somewhat.

This is because the simulation would require an extremely large number of iterations to approach perfect agreement of the time-domain waveforms, which in turn would demand excessive processing times as explained above. (In another iteration, the rise-time of the excitation pulse was set to 0.3 ns with the hope to increase accuracy, but this steeper signal excited higher order modes (TE-modes) which in turn resulted in more peaks and dips of the modeled voltage waveforms.) Despite these small discrepancies, the TOF values obtained from the simulations are in very close agreement to those from the experimental measurements.

The comparison of the measured and simulated results presented in Figure 8 showed the following results:

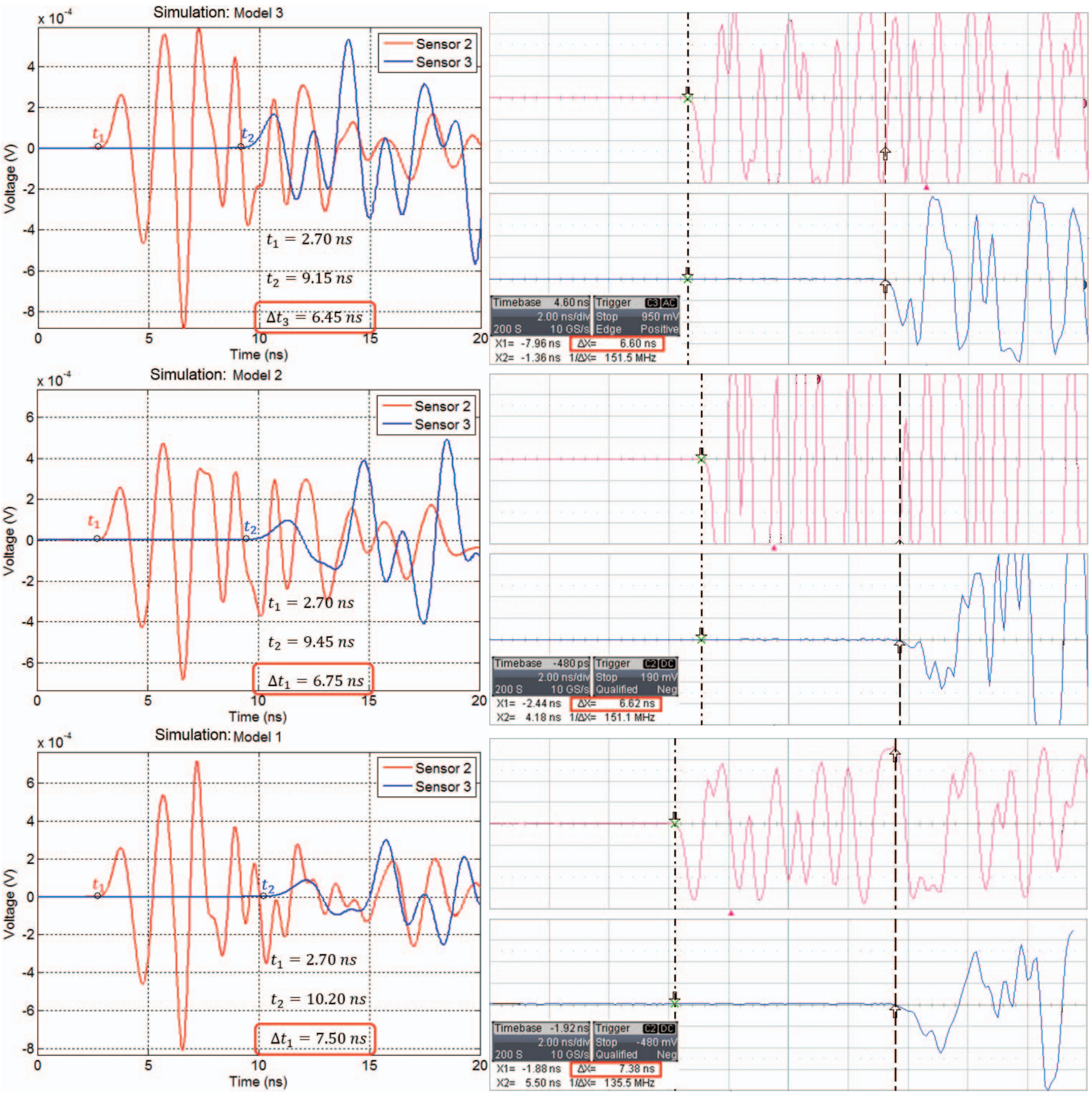

Figure 8. The simulated TOF voltage signals (left) and measured voltage signals (right) are shown. The obtained time-of-flight values reveal an excellent agreement of the simulations with measurements. The obtained waveforms agree also well at the beginning of time in terms of lower propagating modes. The deviation of the measured waveforms from the simulated ones at later times is explained in detail in the text.

- Model 1: TOF-time = 7.38 ns (meas.) and 7.50 ns (sim.)
- Model 2: TOF-time = 6.62 ns (meas.) and 6.75 ns (sim.)
- Model 3: TOF-time = 6.60 ns (meas.) and 6.45 ns (sim.)
- Model 1 – Model 3 = 0.82 ns (meas.) and 1.05 ns (sim.)
- Model 2 – Model 3 = 0.02 ns (meas.) and 0.30 ns (sim.)

The time difference between Model 2 – Model 3 indicates a signal delay effect due to the contact assemblies and the shielding electrodes, which normally accompany each insulator; this value came out to be 0.3 ns. The difference Model 1 – Model 3 reveals the signal delay due to the insulators and shields together, which came out to be 1.2 ns. Thus, the signal delay calculated based on the FEM model due to the insulators is around 0.9 ns which means around 0.9 ns/5=0.18 ns/insulator, only 20 ps different from the actual measurement.

4 ON-SITE OBSERVATION OF DIELECTRIC TIME DELAY EFFECTS

Recently, the authors carried out on-site TOF measurements in order to locate the source of floating-potential type PD signals in a 400 kV GIS which had undergone repairs. Most experienced investigators would expect such a TOF measurement to be straightforward, given the high-amplitude, high pulse-rate characteristics typical of floating-potential PD.

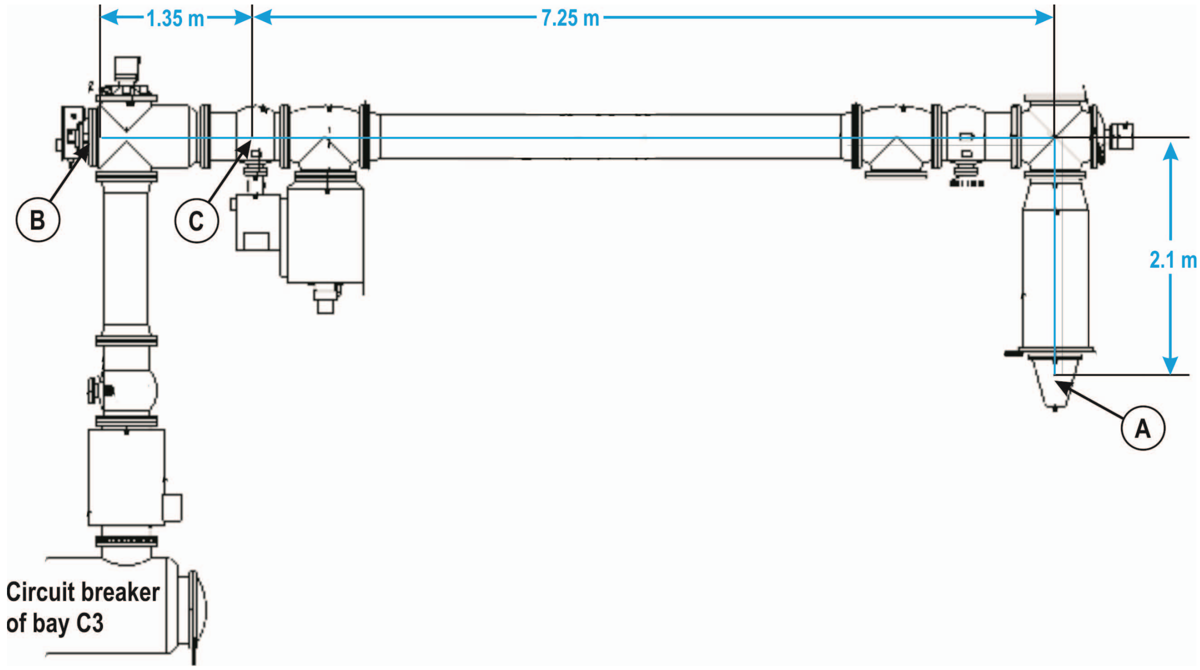

Figure 9. Onsite TOF-measurements on a 420 kV GIS cable feeder is presented. GIS layout and measurement locations are depicted. A: external UHF-PD-sensor at cable sealing end, B: GIS UHF PD sensor C3-PD02, C: shielding of fast acting earth switch.

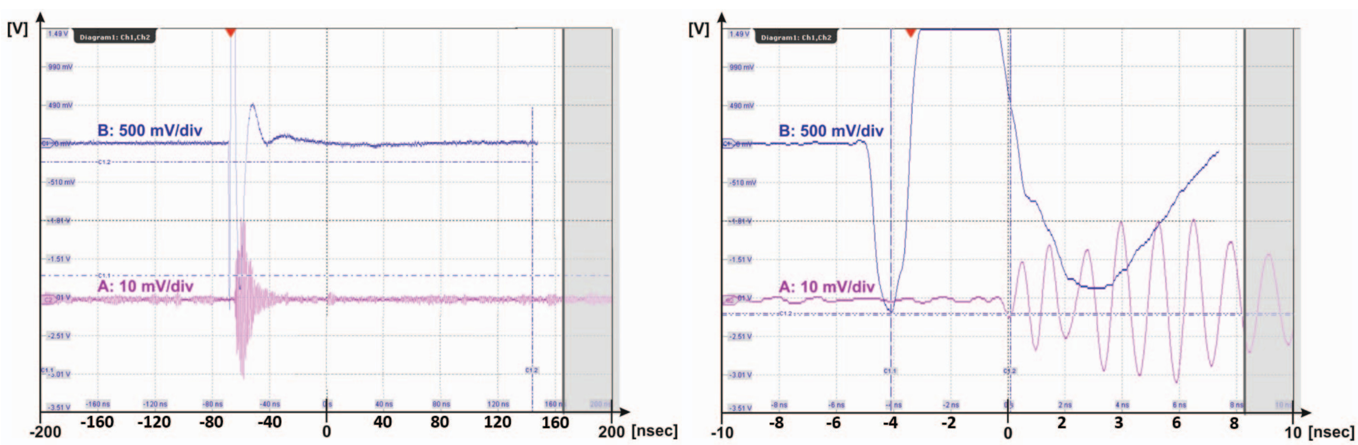

Figure 10. Difference in signal arrival time of measurement channels *A* (red) and *B* (blue). Channel *B* arrives 4.2 ns sooner than channel *A*. The left-hand plot shows the overall pulse shapes; on the right, zoomed in to determine the signal delay ($\Delta t_{KAB} = 4.2\ ns$, the mean value out of 3 measurements).

The following describes a typical on-site TOF measurement performed on the section of GIS shown in Figure 9, consisting of a cable feeder at a 420 kV substation.

By observing the PD signal's dependence on different switching configurations, the rough location of the PD-source was determined to be between the line disconnector switch (location *B*) and the cable termination (location C). Two internal sensors are located at *B* and *C*. In order to measure the entire section under investigation, an external UHF-PD sensor was attached to the cable termination bushing (location *A*).

In a first step, the actual physical distances between the measurement positions *A*, *B* and *C* are measured and verified against the assembly drawings (see Figure 9).

In a second step, the difference in signal transmission time between the measurement chains used at *A*, *B* and *C* are determined. These differences arise from differences in cable lengths, filter delays (if applied), etc. For this measurement, the ends of two measurement chains are connected via a 3 dB signal splitter, and the fast rise-time pulser used to inject signals simultaneously in both branches. Figure 10 shows the result of the measurement of the difference in signal transmission time of the measurement chains *A* and *B*.

In a third step, the overall signal propagation velocity is determined for the entire path, by measuring the signal transmission time between *A* and *C*, using *B* as a signal injection point outside of the measurement path. This is similar to methods used when employing time domain reflectometry (TDR) methods for fault location in HV power cables, and is essentially the methodology we described above to determine the propagation delay of insulators in the measurement path.

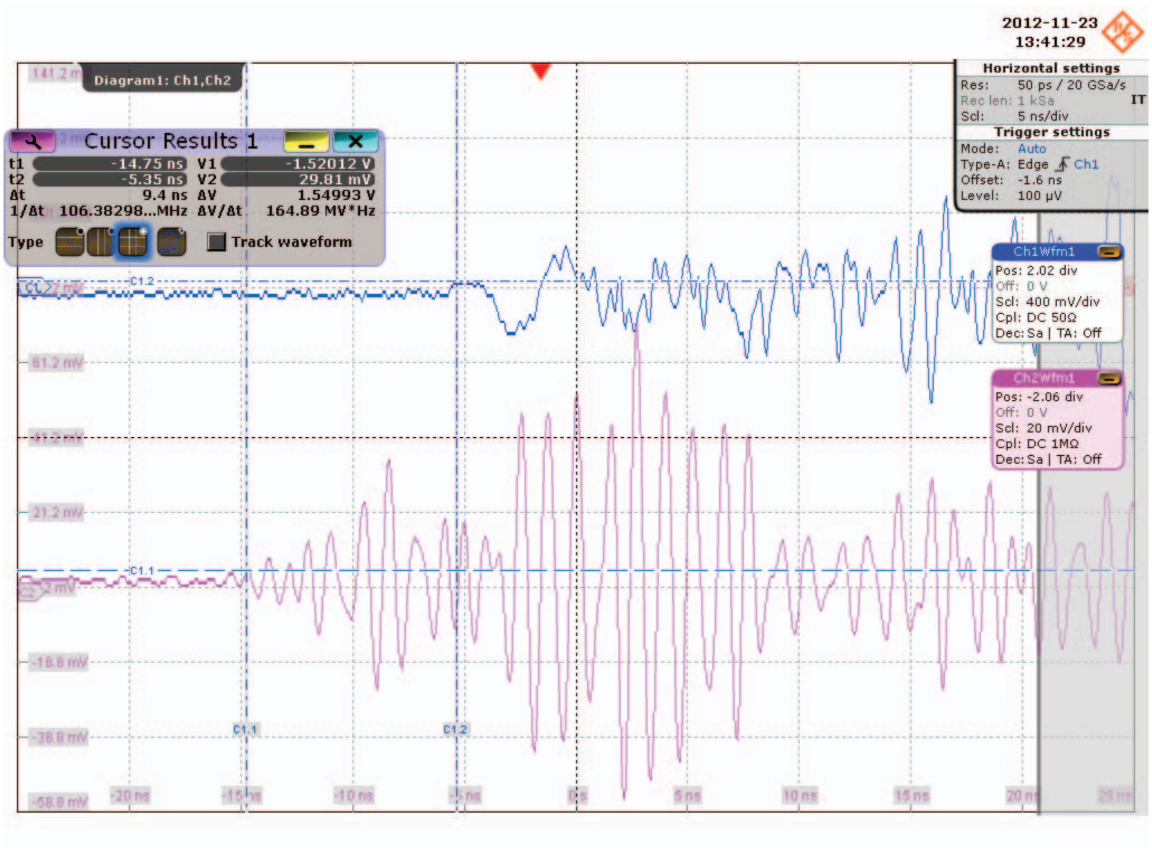

Figure 11. Difference in signal arrival time of the actual PD source measured with channels *A* (red) and *B* (blue) is presented. The cursors – the dotted vertical blue lines labeled 'C1.1' and C1.2' – are set at the beginning of each waveform. Result: t_{PD} = *9.4 ns*; *A* before *B* (mean value out of 3 measurements).

This measurement together with the physical distance and the result of the second step led to a calculated signal propagation velocity of v_{GIS} = 0.226 m/ns.

The propagation velocity thus obtained is considerably lower than the theoretical value *c* usually assumed (0.3 m/ns). There are several reasons for this: (a) the presence of insulators along the TOF path, (b) higher order TE-modes having frequency-dependent propagation velocities (only the TEM mode propagates with the speed of light - 0.3 m/ns.), and (c) the delay effects of the electric shields and their cavities acting as resonators, discussed in the previous section on simulation models.

The fourth step is the determination of the location of the PD source to be removed. Figure 11 shows the result of the measurement at locations *A* and *B*.

Given the actual PD-signal shown in Figure 11, the difficulty in determining the exact starting point of the two incoming signals becomes obvious. Due to noise, filtering, sensor characteristics, etc., the exact signal start can become ambiguous, leading to errors in the difference in arrival times and thus the TOF measurement results. Especially in environments with high levels of external electromagnetic interference (EMI) together with PD signal of low amplitudes, this uncertainty can reach 1 ns or even more; 1 ns is equivalent to 10-20 cm according to (1), depending on the actual propagation velocity.

As a last step, the PD-source location can be calculated. With the difference in signal transmission time between the measurement chains of *A*, *B*: Δt_{KAB} of 4.2 ns (*B* before *A*), the distance between *A* and *B* of 10.7 m, a signal propagation velocity of v_{GIS} = 0.226 m/ns and a result of the TOF measurement of the actual PD-source of t_{PD} = 9.4 ns (*A* arrives before *B*), the distance of the PD-source to the closer measurement location is calculated (based on the principle shown in Figure 1) as follows:

$$l_{xA} = \frac{l_{AB} - v_{GIS}\left(\Delta t_{PD} + \Delta t_{KAB}\right)}{2} \tag{8}$$

As a result, the distance between the PD source and location *A* was calculated to be: $l_{XA} = 3.82\ m$.

The orange region in Fig. 12 shows the location of the PD source as determined by the TOF measurement; based on this result, most experienced investigators would assume the PD source was within the insulator shown or e.g. within its contact assembly. Based on this assumption, the suspect insulator was replaced. However, when high voltage was again applied to the test section, the exact same PD signal re-appeared: somehow the location calculated based on the TOF measurement was slightly incorrect. The same section of the GIS was partially disassembled and the actual PD signal

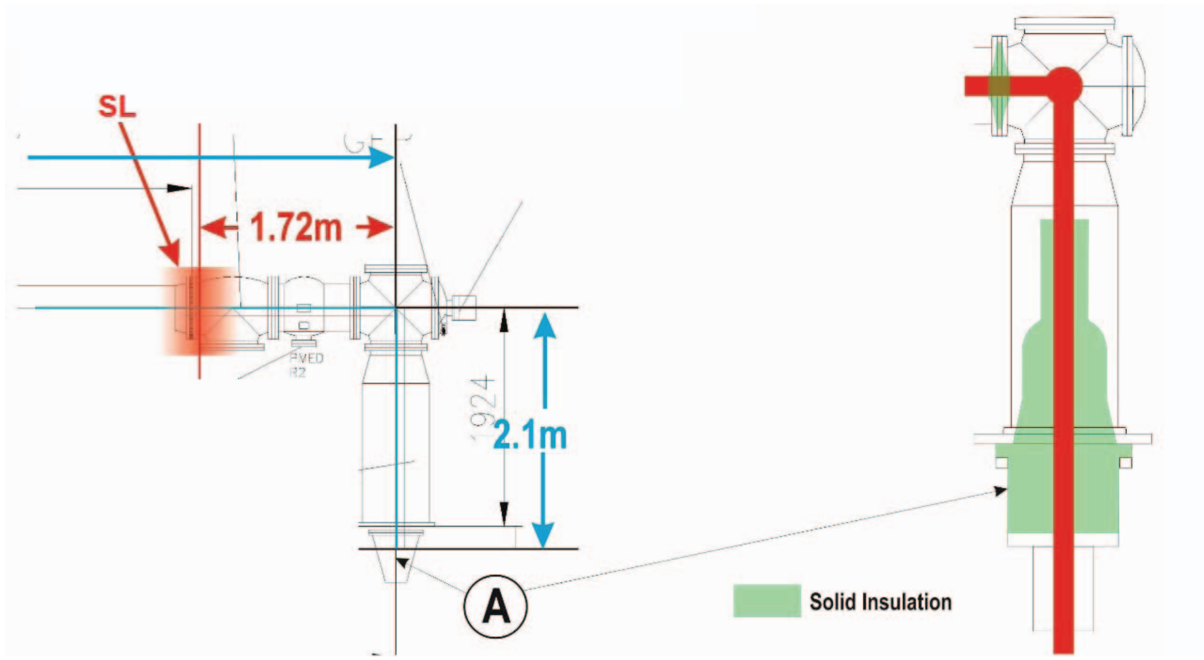

Figure 12. Location of the PD-source is shown. Left side: determined PD-source location based on the TOF measurements; right side: cross section of cable termination with location of measurement point A – illustration of higher content of solid insulation. SL: calculated PD source location on the basis of electric TOF-measurements (phase Y).

source was subsequently found to be a floating shield electrode. The shield was correctly re-installed, after which the PD signal disappeared. This further verified that the TOF calculation had been slightly off.

The exact procedure, set-up, and results of the TOF measurement were examined carefully in an attempt to identify the source of the error. After careful consideration and discussions among the investigators, suspicion began to converge on the external UHF PD sensor installed on the cable bushing, which consists of a massive epoxy-resin insulator. Until now the delay effect of such an insulating structure upon the quantitative results of TOF measurements had not been taken into account. Lacking detailed knowledge of the proprietary construction details of this GIS-cable bushing, it was impossible to guess the exact thickness of the dielectric material through which the PD signal traversed to arrive at the external sensor. However, based on the values for signal delay times in barrier insulators we have described here, any added delay caused by the bushing insulation would tend to 'pull' the calculated position of the PD source based on the TOF measurement toward the cable bushing, i.e. the actual PD signal source, the floating field electrode. This example from an actual field investigation demonstrates that neglecting signal propagation delay effects due to high-dielectric constant insulation materials in a TOF path can result in tangible errors in determining the PD defect's location.

5 CONCLUSIONS

Based on TOF measurements made for the purpose of locating PD sources within GIS, and in particular errors encountered in the case study described above, the authors decided to design a simple experiment to verify whether the influence of high-dielectric constant insulation materials on the velocity of propagation was significant and measurable. The results of the experiment determined that it was. Further, a sophisticated electromagnetic propagation model of the test set-up was created in order to precisely simulate the experimental measurements. A comparison of the actual measurements with the simulations revealed very close agreement.

Along with the delay effects described above, an additional factor which strongly influences TOF measurement accuracy is the signal-to-noise ratio (SNR) of the measured signals. The measurements and simulated signals shown here are all virtually free of external interference, but this is often not the case on site. The presence of external noise can have a significant effect on the difference in time-of-arrival because the investigator will find it difficult to discern the exact time at which the PD signal climbs out of the background noise. Indeed, the small differences between the TOF time intervals from the experimental measurements and the modelled simulations described here can in part be attributed to small variations in placement of the cursors on the oscilloscope. The authors intend on exploring the effects of poor SNR and other issues affecting TOF measurement outcomes in future work.

In terms of practical TOF measurements on GIS, especially on long or complicated geometries or sections containing dielectric insulation components with high values of ε, engineers carrying out TOF measurements on GIS should probably take extra precaution to carefully account for the number, type (composition i.e. dielectric constant of the material), and shapes of dielectric components along the TOF path. A good example would be where there are different numbers and combinations of barrier and support insulators between the PD signal source and the sensors at which the TOF signals are being acquired. As shown here, when the TOF measurement path includes even relatively short differential distances through high-dielectric constant materials, these can result in signal delay effects which can lead to a false location determination.

ACKNOWLEDGEMENTS

The authors wish to thank Mirko Momcilovic and Fabio Mehltretter for their kind assistance with the CAD drawings, and Mr. Albert Spoegler for help with graphics.

REFERENCES

[1] S.A. Boggs, “Electromagnetic Techniques for Fault and Partial Discharge Location in Gas-Insulated Cables and substations”, IEEE Trans. Power App. Syst., Vol. 101, pp. 1935-1941, 1982.
[2] B. F. Hampton and R.J. Meats, “Diagnostic Measurements at UHF in Gas Insulated Substations”, IEE Proc., Vol. 135, part C, No. 2, pp. 137-144, 1988.
[3] J.S. Pearson, O. Farish, B.F. Hampton, M.D. Judd, D. Templeton, B.M. Pryor and I. Welch, “Partial Discharge Diagnostics for Gas Insulated Substations”, IEEE Trans. Dielectr. Electr. Insul.., Vol. 2, No. 5, pp. 893-905, 1995.
[4] CIGRE WG D1.33, Tech. Brochure 444, "Guidelines for Unconventional Partial Discharge Measurements", 2010.
[5] CIGRE WG D1.33, Tech. Brochure 502, "High-Voltage On Site Testing with Partial Discharge Measurement", 2012.
[6] IEC 62478, "High-voltage test techniques – Measurement of partial discharge by electromagnetic and acoustic methods", publication pending, 2015.
[7] S. M. Hoek, “Teilentladungsortung in gasisolierten Schaltanlagen im Frequenzbereich“, ETG "Diagnostik elektrotechnischer Betriebsmittel" Kassel, 2006 (in German).
[8] S. Hoek, M. Bornowski, S. Tenbohlen, T. Strehl and U. Riechert, “Partial discharge detection and localization in gas-insulated switchgears“, Stuttgarter Hochspannungs symposium, pp. 211-218, 2008.
[9] E. Kuffel, W.S. Zaengel, J. Kuffel, *High Voltage Engineering Fundamentals*, 2nd Ed., ISBN 0 750636343, Butterworth-Heinemann, 2000.
[10] J. D. Jackson, *Classical Electrodynamics*, Third Edition, John Wiley & Sons, New York, 1998.
[11] J. Smajic, W. Holaus, J. Kostovic and U. Riechert, “3D Full-Maxwell Simulations of Very Fast Transients in GIS”, IEEE Trans. Magnetics, Vol. 47, No. 5, pp. 1154-1517, 2011.
[12] COMSOL Multiphysica Modeling Software, www.comsol.com, 2015.
[13] H. Gremmel, G. Kopatsch 2006 *ABB Schaltanlagen Handbuch* (Cornelsen Verlag Scriptor GmbH & Co.)
[14] J. W. Schmidt and M. R. Moldover, “Dielectric Permittivity of Eight Gases Measured with Cross Capacitors”, Int’l. J. Thermophysics, Vol. 24, No. 2, 2002.

Glenn Behrmann (S’78, M’79) received a B.S.E.E. degreefrom Union College, Schenectady, NY, in 1979. He began working in RF engineering and signal processing at MIT Lincoln Laboratory in Lexington, MA, USA. He continued in RF and EMC, joining ABB Corporate Research in Baden, Switzerland in 1989. At ABB his work focuses on detection, monitoring, and assessment of PD signals in GIS. He has authored papers and holds patents in the field, and is active in CIGRE and IEC.

Kris Wyss, born in Zurich, Switzerland attained the Dipl. Energy Technician HF degree from the ABB Technical School in Baden in 2014. As part of his thesis “Automated location of partial discharge in GIS”, he carried out the laboratory measurements whose results are published in this paper. He has been with ABB since 2007 and since 2013 active in quality assurance, focusing on high-voltage testing and partial discharge measurement in GIS.

Jonas Weiss earned a Diploma as Energy Technician at the ABB Technical School in Baden (CH) and is with ABB Traction Systems in Turgi since 2015. As part of his thesis on "Automated location of partial discharge in GIS", he carried out several of the TOF measurements whose results are published in this paper.

Markus Schraudolph studied communications engineering at GBS Munich and electrical power engineering at the University of Applied Sciences Konstanz. He has wide experience in high voltage and PD testing, both on site and in the laboratory. Since 2010 he is Head of Test Technology & Routine Test at ABB High Voltage Technologies in Zürich.

Stefan M. Neuhold received his Diploma in electrical engineering and the PH. D. degree from the Swiss Federal Institute of Technology (ETH) in Zurich, Switzerland, in 1993 and 2007, respectively. In 1993 he began working as test engineer at ABB high voltage technology in Zürich. From 1994 to 1998 he was Manager for high voltage testing of GIS (factory and on site) and involved in the practical implementation of UHF-PD-measurement for GIS on site. From 1998 to 2001 and since 2006 he is a test engineer and manager of R & D projects at the independent research and testing commission FKH in Switzerland with specialization on GIS testing and diagnosis. Since 1993 he commissioned more than 100 GIS substations in the voltage range between 24 kV up to 550 kV. His current interests include UHF PD-signal measurement and characterization as well as diagnosis of vintage GIS substations. He is member of several working groups of CIGRE and author of papers dealing with GIS testing. Dr. Neuhold received the innovation prize of the Swiss energy technical society (ETG) in 2005.

Jasmin Smajic (M‘07) received his M.Sc. and Ph.D. degrees from the Faculty of Electrical Engineering and Computing in Zagreb (Croatia) in 1998 and 2001, respectively, on the topic of numerical computing and optimization of static and time-varying electromagnetic fields. From 2002 to 2004 he was a postdoctoral research fellow in the Laboratory for Electromagnetic Fields and Microwave Electronics at the ETH Zurich (Switzerland). The main topics of his post-doctoral studies were full-Maxwell electromagnetic simulations of photonic crystals and similar electromagnetic meta-materials. In 2004 he took a position of scientist at the ABB Corporate Research Centre in Baden-Dättwil (Switzerland) where he stayed until 2011. His work in ABB covered a wide range of projects in the field of computational and applied electromagnetics such as LI-modeling and simulation of transformer windings, fast electromagnetic transients in power- and distribution transformers, coupled electromagnetic-mechanical and electro-magnetic-thermal analysis of transformers and circuit breakers, and very fast electromagnetic transients in gas insulated switchgears. In 2011, he was appointed professor of electrical engineering at University of Applied Sciences Eastern Switzerland (HSR). Jasmin Smajic is a member of CIGRE and he has authored over hundred scientific publications, several books, and dozens of patents.